Decadal Variability in the Formation of the North Pacific Subtropical Mode Water: Oceanic versus Atmospheric Control

BO QIU AND SHUIMING CHEN

Department of Oceanography, University of Hawaii at Manoa, Honolulu, Hawaii

(Manuscript received 31 March 2005, in final form 15 November 2005)

ABSTRACT

In situ temperature and altimetrically derived sea surface height data are used to investigate the low-frequency variations in the formation of the North Pacific Ocean Subtropical Mode Water (STMW) over the past 12 yr. Inside the Kuroshio Extension (KE) recirculation gyre where STMW forms, the dominant signal is characterized by a gradual thinning in the late winter mixed layer depth and in the 16°–18°C thermostad layer from 1993 to 1999 and a subsequent steady thickening of these features after 2000. This same decadal signal is also seen in the low-potential-vorticity (PV) STMW layer in the interior subtropical gyre south of the recirculation gyre. By analyzing the air–sea flux data from the NCEP–NCAR reanalysis project, little correlation is found between the decadal STMW signal and the year-to-year changes in the cumulative wintertime surface cooling. In contrast, the decadal signal is found to be closely related to variability in the dynamic state of the KE system. Specifically, STMW formation is reduced when the KE path is in a variable state, during which time high regional eddy variability infuses high-PV KE water into the recirculation gyre, increasing the upper-ocean stratification and hindering the development of a deep winter mixed layer. A stable KE path, on the other hand, favors the maintenance of a weak stratification, leading to a deep winter mixed layer and formation of a thick STMW layer. The relative importance of the surface air–sea flux forcing versus the preconditioning stratification in controlling the variations in the late winter mixed layer depth is quantified using both a simple upper-ocean heat conservation model and a bulk mixed layer model. The majority of the variance (~80%) is found to be due to the stratification changes controlled by the dynamic state of the KE system.

1. Introduction

Because of the large thermal inertia carried by the ocean, long-term changes in the water masses of the upper ocean have attracted increasing attention for studies of the midlatitude climate system. In the western North Pacific Ocean, a prominent, upper-ocean water mass is the Subtropical Mode Water (hereinafter STMW) formed on the southern side of the Kuroshio and Kuroshio Extension (e.g., Masuzawa 1969, 1972; Suga et al. 1989; Bingham 1992; Suga and Hanawa 1995a; Hanawa and Talley 2001). Characterized by a layer of minimum temperature gradient (i.e., thermostad) in between the seasonal and permanent thermoclines, STMW is a product of wintertime convective cooling. Sheltered from surface processes in subsequent seasons or years, depending on the atmospheric and oceanic conditions, STMW can serve as a sequestered heat reservoir that will reemerge through vertical entrainment and/or lateral induction, modulating local or remote wintertime sea surface temperatures (SSTs).

Several data analysis studies in the past have shown that the formation of STMW in the western North Pacific exhibited significant interannual to decadal variations. For example, Bingham et al. (1992) found that STMW was thicker and more uniform in temperature during 1938–42 than during 1978–82; they attributed this difference to the stronger wintertime cooling during the 1938–42 pentad. Based on repeat hydrographic surveys along the 137°E meridian south of Japan, Suga and Hanawa (1995b) found a good correlation between the observed STMW properties and the surface pressure difference between Nemuro, Japan, and Irkutsk, Russia, which serves as an index for the strength of the wintertime East Asian monsoon. The fact that a more intense monsoon results in the formation of a deeper mixed layer and thicker and colder STMW has also

Corresponding author address: Dr. Bo Qiu, Dept. of Oceanography, University of Hawaii at Manoa, 1000 Pope Rd., Honolulu, HI 96822.
E-mail: bo@soest.hawaii.edu

been stressed in other recent studies by Yasuda and Hanawa (1999), Taneda et al. (2000), and Hanawa and Kamada (2001).

While many previous studies of STMW have stressed the importance of atmospheric forcing, it is worth emphasizing that the STMW formation and its subsequent evolution also depends on conditions of the oceanic circulation, such as the preexisting density stratification and the level of mesoscale eddy activity. In their respective studies of the 18° Water variability at the *Panulirus* station in the subtropical North Atlantic, for example, Talley and Raymer (1982) and Jenkins (1982) found little correspondence between the changes in the wintertime surface heat flux forcing and the observed 18° Water properties. Talley and Raymer suggested that the observed 18° Water property changes may be related to the variability of the Gulf Stream recirculation gyre. By combining satellite altimetry data and subsurface temperature data, Dong (2004) found that thicker (thinner) 18° Water was formed when the Gulf Stream recirculation gyre was weaker (stronger). Dong suggested that this interannual variability in the 18° Water thickness was related to the lateral heat convergence in the upper ocean. In the subtropical North Pacific, Yasuda and Hanawa (1997) observed warming in the southwestern part of STMW after the mid-1970s. They suggested that this decadal warming was likely caused by increased advection of warm water by the Kuroshio.

Following the launch of the Ocean Topography Experiment (TOPEX)/Poseidon altimetry mission in 1992, our ability to observe the time-varying surface ocean circulation and the mesoscale eddy field has improved significantly. During the past 12 yr, the Kuroshio Extension (KE) jet and its southern recirculation gyre have been observed to oscillate between two dynamically distinct states. As indicated by the yearly distributions of the KE paths in Fig. 1, the KE jet was relatively stable in 1993–94, but made a transition to a more variable state after mid-1995. This transition can also be seen in Fig. 2, which shows the time series of the KE pathlength and the eddy kinetic energy level in the region of 32°–38°N and 141°–153°E. The KE jet returned to the stable state in January 2002. In the past 3 yr, the KE jet has been accompanied by an intensified recirculation gyre, and the level of the regional mesoscale eddy variability has remained relatively low.

Because STMW is formed in the recirculation gyre adjacent to the KE jet, it is natural to ask to what extent the decadal changes observed in the KE system can affect the formation of STMW. The objective of the present study is to address this question by analyzing available water temperature data from 1992 to 2004 in the STMW formation region, as well as an interior region south of the KE recirculation gyre. By focusing on both the surface air–sea flux forcing and the preconditioning associated with the different dynamic states of the KE jet and the recirculation gyre, we attempt to quantify the relative importance of the oceanic versus the atmospheric control over the low-frequency STMW changes observed in the last 12 yr.

At present, a collaborative research program, named the Kuroshio Extension System Study (KESS), is under way. One of the goals of KESS is to clarify processes that govern the temporal variability of STMW and its impact upon the sea surface temperature and surface mixed layer (Qiu et al. 2006). While much will be learned about STMW from the 2-yr, dedicated field measurements, a careful analysis such as that presented in this study will help to interpret the finescale KESS results in the context of the lower-frequency variability of the KE system and STMW.

This paper is organized as follows. Section 2 provides a brief description of the water temperature, the sea surface height, and the surface air–sea flux datasets used in this study. In section 3, we focus on the observed variability of STMW in its formation region within the KE recirculation gyre. STMW variability *south* of the recirculation gyre is analyzed in section 4. In section 5, we examine the relationships between the observed STMW changes, the surface net heat flux forcing, and the variability in the dynamic state of the KE system. The effects of lateral oceanic advection are explored in section 6. A more quantitative analysis on the relative importance of the oceanic versus atmospheric forcing is pursued in section 7 with the aid of a bulk mixed layer model. Section 8 summarizes the results from this study.

2. Data

The water temperature data used in this study consist of the salinity/conductivity–temperature–depth (S/CTD) and expandable bathythermograph (XBT) data in the *World Ocean Atlas 2001* (*WOA01*; Conkright et al. 2002). The *WOA01* dataset is supplemented by temperature data archived by the Japan Oceanographic Data Center (http://www.jodc.go.jp) and by profiling float CTD data from the International Argo Program (Argo Science Team 2001). Inclusion of the Argo float CTD data greatly improves the data coverage in the years after 1999. For data quality control, we first remove duplicate profiles in the different data sources. For each temperature profile, the measured temperature data are compared with the $1° \times 1°$ *WOA01* clima-

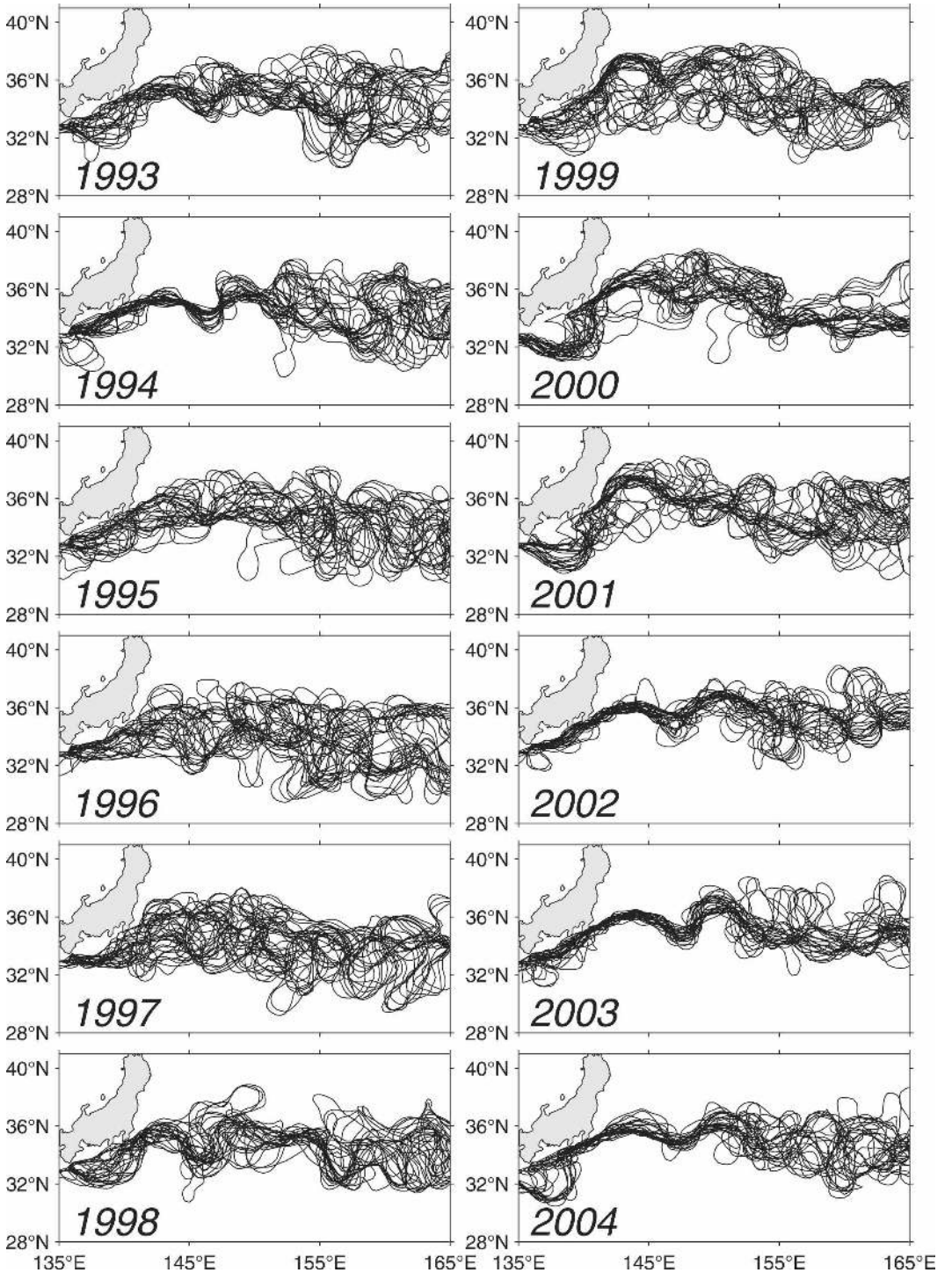

FIG. 1. Yearly maps of the biweekly KE jet paths derived from the merged satellite altimetry data. Individual paths correspond to the 1.7-m contours in the weekly SSH field (adapted from Qiu and Chen 2005).

tology, $T_{\text{clim}}(z)$. Data are excluded if they fall outside of the 2 standard deviation envelopes of $T_{\text{clim}}(z)$. Profiles with large temperature inversions ($dT/dz < -0.1$°C m^{-1}) are also removed from the analysis. After the profile passes the quality control procedure, the temperature data are interpolated onto a regular 10-m vertical grid between the surface and the 450-m depth.

Satellite altimetry data are used in this study to cap-

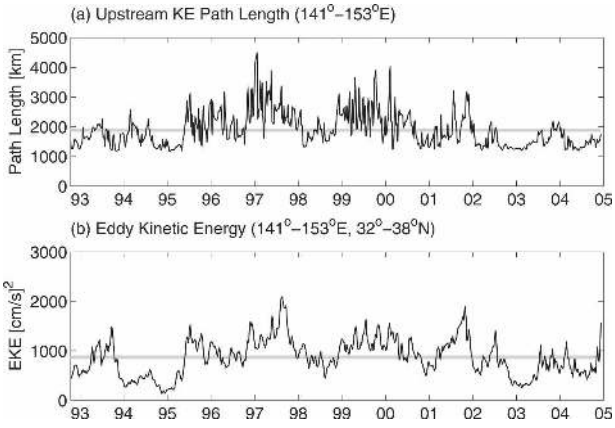

FIG. 2. (a) The KE pathlength integrated from 141° to 153°E. (b) The level of eddy kinetic energy averaged in the upstream KE region of 32°–38°N and 141°–153°E. Gray lines denote the mean values over the period of analysis. Both of the time series are derived from the merged satellite altimetry data (see Qiu and Chen 2005).

ture the time-varying surface dynamic signals surrounding the KE-recirculation gyre region. For this purpose, we use the global sea surface height (SSH) anomaly dataset compiled by the Space Oceanographic Division of the CLS Corporation near Toulouse, France. The dataset merges the TOPEX/Poseidon, *Jason-1*, and *European Remote Sensing Satellites 1* and *2* (*ERS-1/2*) along-track SSH measurements and has a much improved capability of detecting the mesoscale SSH signals (Le Traon and Dibarboure 1999; Ducet et al. 2000). The CLS SSH dataset has a 7-day temporal resolution, a 1/3° × 1/3° spatial resolution, and covers the period from October 1992 to December 2004. For the mean SSH field, we adopt in this study the surface dynamic height (0/1000 dbar) climatology compiled by Teague et al. (1990).

The daily surface air–sea flux data from the National Centers for Environmental Prediction–National Center for Atmospheric Research (NCEP–NCAR; Kistler et al. 2001) reanalysis are used in this study to quantify the wintertime atmospheric forcing over the STMW formation region. Using the surface meteorological data measured by a Japan Meteorological Agency buoy at 29°N, 135°E, we recently carried out an in-depth comparison between the daily NCEP–NCAR air–sea flux product and the buoy estimate (Qiu et al. 2004). The rms amplitude of the NCEP–NCAR net heat flux (Q_{net}) was found to be biased high by 23%. Despite this amplitude bias, however, the NCEP–NCAR product captures the timing and relative strength of the synoptic-scale Q_{net} forcing very well. Little bias was found between the daily surface wind stress data in the NCEP–NCAR reanalysis and the buoy estimate. Based on these findings, the magnitude of the NCEP–NCAR heat flux data used in this study is scaled down by applying a multiplicative factor of 0.813. No adjustment is made to the daily NCEP–NCAR wind stress data.

3. Decadal STMW changes in the KE recirculation gyre region

Results from the synoptic CTD and profiling float surveys of the KESS cruise in June 2004 reveal that the STMW formation region, defined as where STMW is in direct contact with the late winter surface layer, is geographically confined to the KE recirculation gyre north of ~30°N (Qiu et al. 2006). South of this southern boundary, low potential vorticity waters with temperatures of 16°–18°C do not outcrop locally and are advected from the formation region to the north. In this section we will focus on the STMW variability in its formation region. Variations in STMW south of the recirculation gyre are examined in section 4.

For the study of STMW variability, one would ideally like to form a gridded monthly dataset of the three-dimensional temperature field. Sparsity of in situ data, unfortunately, precludes us from taking this approach. Figure 3, for example, shows the locations of the temperature profiles available in 1999 (the distribution is typical for the other years as well). Even with a coarse 2° × 2° grid, it would be difficult to map out the monthly temperature field without significant data gaps. Another factor that goes against a mapping procedure is that the KE is an inertial jet accompanied by frequent large-amplitude meanders and cutoff mesoscale eddies [e.g., Mizuno and White (1983); see also Fig. 1]. In the example shown in Fig. 3, a cold-core eddy with a radius of ~150 km can be seen to reside near 34°N and 144°E. Sequential SSH maps (not shown) indicate that this cold-core eddy originated north of the unstable KE jet. As evidenced by the blue colors in Fig. 3, waters within this cold-core eddy have shallow thermocline depths and are devoid of thermostad features.[1] A simple spatial gridding is likely to artificially mix water masses, obscuring the time-varying STMW signals of interest to us.

Given these issues, we examine the STMW within the recirculation gyre by forming a single time series of $T(z, t)$. Specifically, $T(z, t)$ is constructed by first grouping the available temperature profiles into individual

[1] The correspondence between the SSH values and the 17°C isotherm depths in Fig. 3 is marginally favorable because it is a yearly picture and because 1999 was when the KE system was in an unstable state (Fig. 1). The correspondence improves significantly if these two quantities are plotted on a monthly basis.

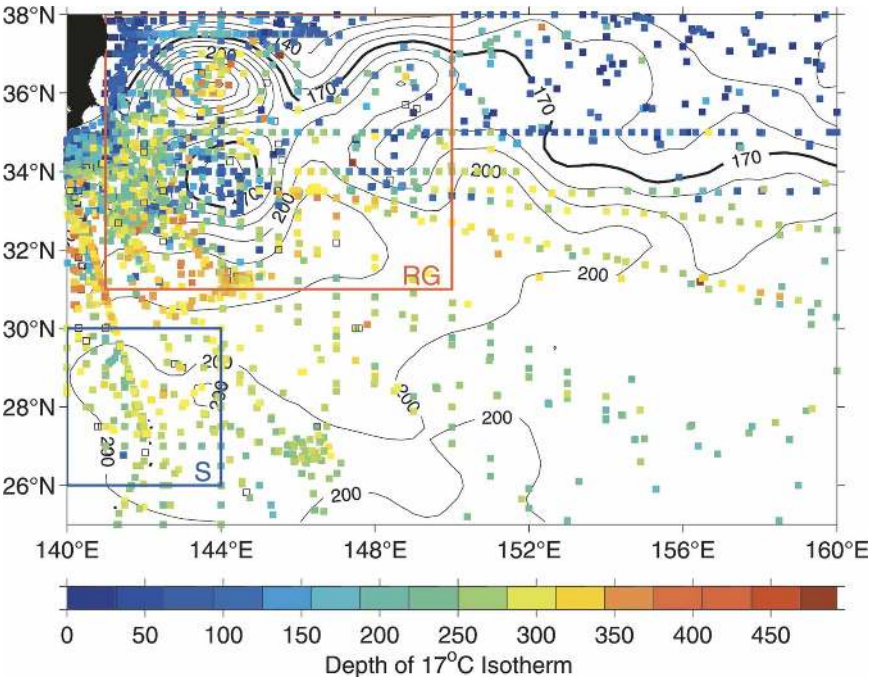

FIG. 3. Locations of temperature profiles available in 1999 around the KE and its recirculation gyre regions. Colors denote the depth of the 17°C isotherm detected in the individual profiles. Contours represent the mean SSH field in 1999 from satellite altimetry measurements (cm). The two boxes denote the areas in which the monthly $T(z, t)$ profiles are constructed.

months. Within each month (from October 1992 to December 2004), each profile in the region of 31°–38°N and 141°–150°E (the RG box in Fig. 3) is compared with the collocated, weekly SSH value from the altimetry measurements. The profile is regarded as within the recirculation gyre if the corresponding SSH value exceeds 2.0 m. Use of this threshold SSH value ensures that the profiles inside the KE jet and cutoff cold-core rings are excluded (choosing a lower threshold value, e.g., 1.9 m, will not alter the results presented in this study). The single temperature profile $T(z, t)$ is finally obtained by averaging all profiles that fall within the recirculation gyre box.

Figure 4a shows the time series of $T(z, t)$ following the procedures described above. The black line in the figure denotes the base of the mixed layer, defined as where the water temperature drops by 0.5°C from the surface value. Based on the $T(z, t)$ profiles, Fig. 4b shows the monthly time series of potential vorticity (PV):

$$Q(z, t) = f\alpha \frac{\partial T(z, t)}{\partial z}, \qquad (1)$$

where f is the Coriolis parameter and α is the thermal expansion coefficient of seawater. Notice that many previous studies have used $\partial T/\partial z = 1.5°\text{C}\ (100\ \text{m})^{-1}$ as a criterion for identifying STMW (e.g., Hanawa and Talley 2001). In Eq. (1), this $\partial T/\partial z$-based criterion corresponds to a threshold PV value of $Q = 2.5 \times 10^{-10}$ $\text{m}^{-1}\ \text{s}^{-1}$. From Fig. 4, it is clear that both the late winter mixed layer depth and the low-PV STMW layer underwent significant decadal changes over the past 12 yr. Accompanied by deep winter mixed layers, STMW with $Q < 2.5 \times 10^{-10}\ \text{m}^{-1}\ \text{s}^{-1}$ abounded in 1993–96. In contrast, shallow mixed layers persisted during winters from 1998 to 2000 and there existed little thermostad water with $Q < 2.5 \times 10^{-10}\ \text{m}^{-1}\ \text{s}^{-1}$ during that period beneath the seasonal thermocline. From 2001 to 2004, there has been a gradual increase in the depth of the winter mixed layer, as well as the amount of low-PV STMW.

The decadal signals revealed in Fig. 4 can also be captured if we simply plot out the time series of the 16°–18°C layer thickness from the $T(z, t)$ profiles (see Fig. 5). Besides the large spikes seen in several winters, Fig. 5 reveals that the STMW layer thickness underwent a decadal oscillation similar to those seen in the winter mixed layer depth and $Q(z, t)$ time series: the layer was thick, ~150 m, in 1993–94 and decreased to a minimum of ~100 m in 1998–99. A gradual increase in

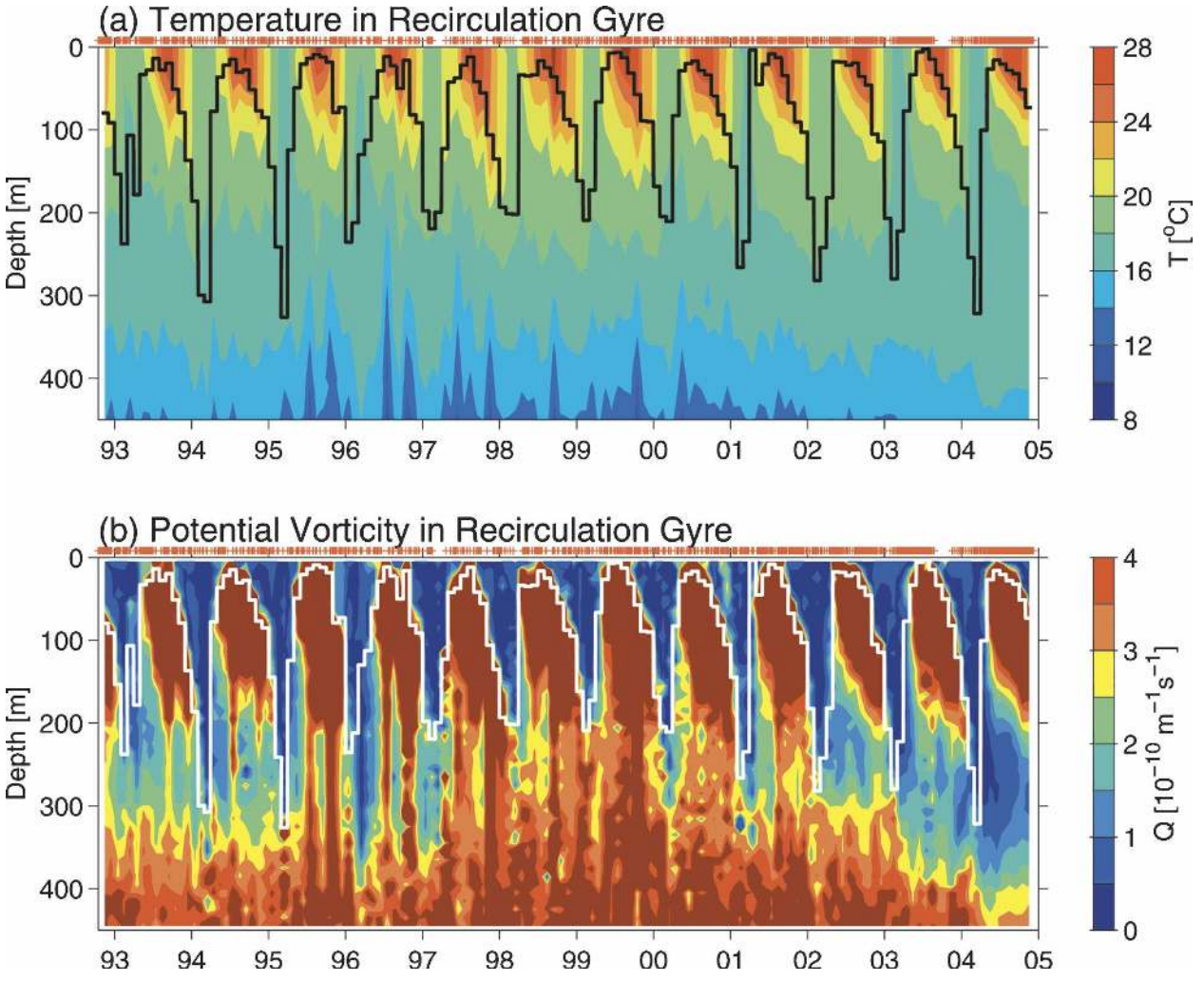

FIG. 4. Monthly time series of (a) temperature and (b) potential vorticity averaged over the RG box shown in Fig. 3. The thick black and white lines in (a) and (b) denote the base of the mixed layer, defined as where the temperature drops by 0.5°C from the surface value. Red crosses indicate the individual temperature profiles used in constructing the monthly $T(z, t)$ profiles.

layer thickness is seen after 2001, with the layer thickness exceeding 200 m in 2004. The large spikes in layer thickness seen in Fig. 5 reflect the wintertime outcropping of the 16°–18°C layer to the sea surface. It is not surprising that the outcropping occurs in winters when the STMW layer in the subsequent seasons has a large thickness.

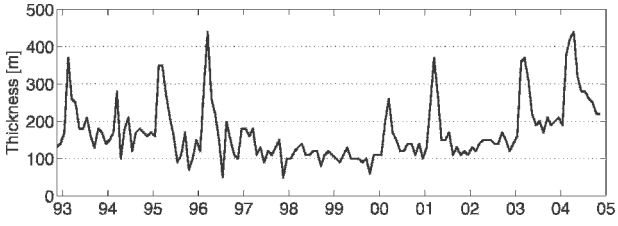

FIG. 5. Time series of the 16°–18°C layer thickness in the recirculation gyre region. Based on the $T(z, t)$ profiles shown in Fig. 4a.

Because of limitations of the spatial data coverage, we have restricted our analysis above of STMW to a single time series $T(z, t)$ in the recirculation gyre. To demonstrate that this time series is representative of a broader region of the recirculation gyre, we plot in Fig. 6 the vertical temperature sections from two XBT transects across the KE recirculation gyre in June 2000 and June 2004, respectively. Consistent with the results presented in Fig. 5, the STMW thickness (represented in Fig. 6 by the shaded 16°–18°C layer) is larger in the 2004 transect than in the 2000 transect. Notice that the difference in the STMW thickness between these two transects extends over a large zonal distance from 142° to 170°E. This implies that the decadal signals seen in

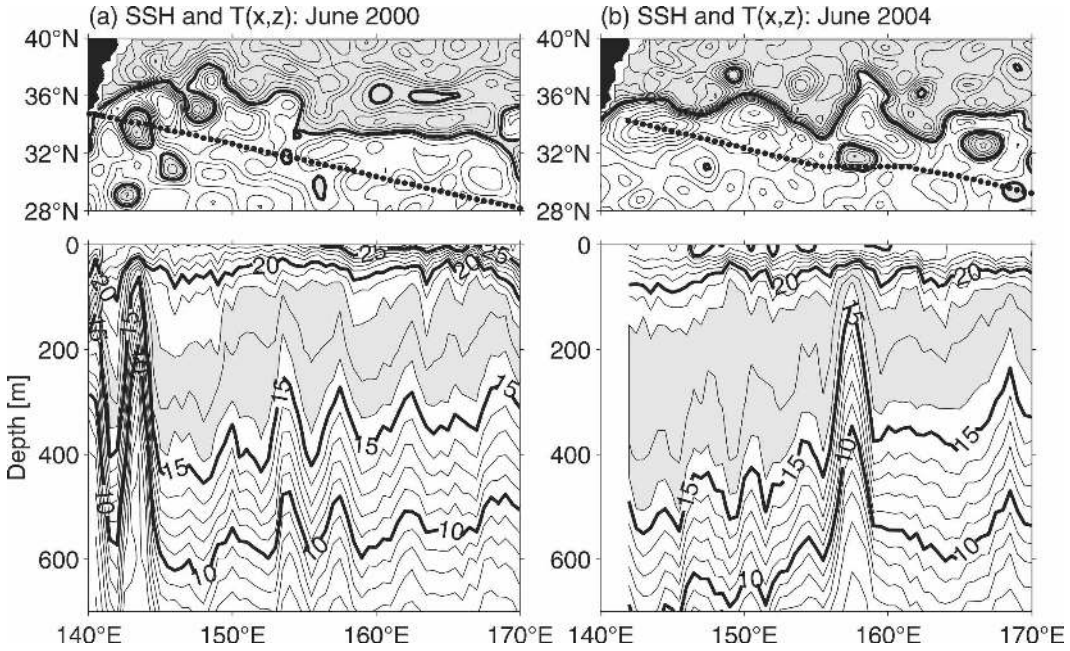

FIG. 6. Vertical temperature sections across the KE recirculation gyre in (a) June 2000 and (b) June 2004. (top) Black dots indicate positions of XBT casts and contours denote the concurrent SSH field. Contour interval for the SSH field is 0.1 m and thick lines denote the 1.7-m contours. Areas where SSH <1.7 m are shaded. (bottom) Contour intervals for the isotherms are 1°C. Areas where 16°C < T < 18°C are shaded.

Figs. 4 and 5 is representative of conditions of a broader region south of the KE jet.

4. STMW changes south of the recirculation gyre

Before examining the causes for the observed STMW changes in the recirculation gyre, it is useful to clarify the relationship between the STMW changes observed in its formation region (i.e., the KE recirculation gyre) and those in the interior of the subtropical gyre. Lack of information about the time-varying KE state has prompted many studies of STMW in the past to focus on the STMW signals south of the recirculation gyre, where the circulation is less perturbed by the KE jet meanders and large-amplitude mesoscale eddies. For this study, we will specifically focus on an area encompassed by 26°–30°N and 140°–144°E (i.e., box S in Fig. 3). This area is chosen both because it is in the pathway of the subducted STMW formed in the recirculation gyre (e.g., Bingham 1992; Huang and Qiu 1994; Suga and Hanawa 1995a) and because it has an uninterrupted distribution of monthly temperature profiles. In fact, this area was the focus of a recent study by Taneda et al. (2000), in which they analyzed the STMW variability for the period from 1984 to 1995. For our analysis, we will cover the period from 1992 to 2004 and discuss the results in light of the findings presented in the preceding section.

Figure 7 shows the time series of $T(z, t)$ and $Q(z, t)$ derived from all available temperature profiles in box S (unlike the RG box, no SSH threshold is used for this box). In the box, STMW, as represented by the 16°–18°C layer, resides in the depth range of 175–325 m. A look at the $Q(z, t)$ profiles in this depth range reveals a decadal signal very similar to that detected in Fig. 4b, namely, values of PV were high in 1998–2001, and low before 1997 and after 2002. Indeed, as plotted in Fig. 8, the low-frequency changes in the 16°–18°C layer thickness in this southern box reflect very much the decadal thickness changes of this same layer in the recirculation gyre (cf. Fig. 5). Dynamically, this is to be expected. As can be confirmed in Fig. 7a, the 16°–18°C layer does not outcrop locally in box S and the low-PV STMW water detected in this box is shielded from the regional surface atmospheric forcing. In this case, as may be expected from ventilated thermocline theory (Luyten et al. 1983; Talley 1985), changes in the 16°–18°C layer thickness should reflect the changes in its outcropping region in the KE recirculation gyre.

One important point worth noting in Fig. 7 is that the winter mixed layer depth in the southern box showed little decadal variations in the past 12 yr. This is in sharp contrast to the recirculation gyre where the observed mixed layer depth had a clear decadal modulation in connection with the changes in the STMW layer thickness (see Fig. 4a). As the atmospheric forcing com-

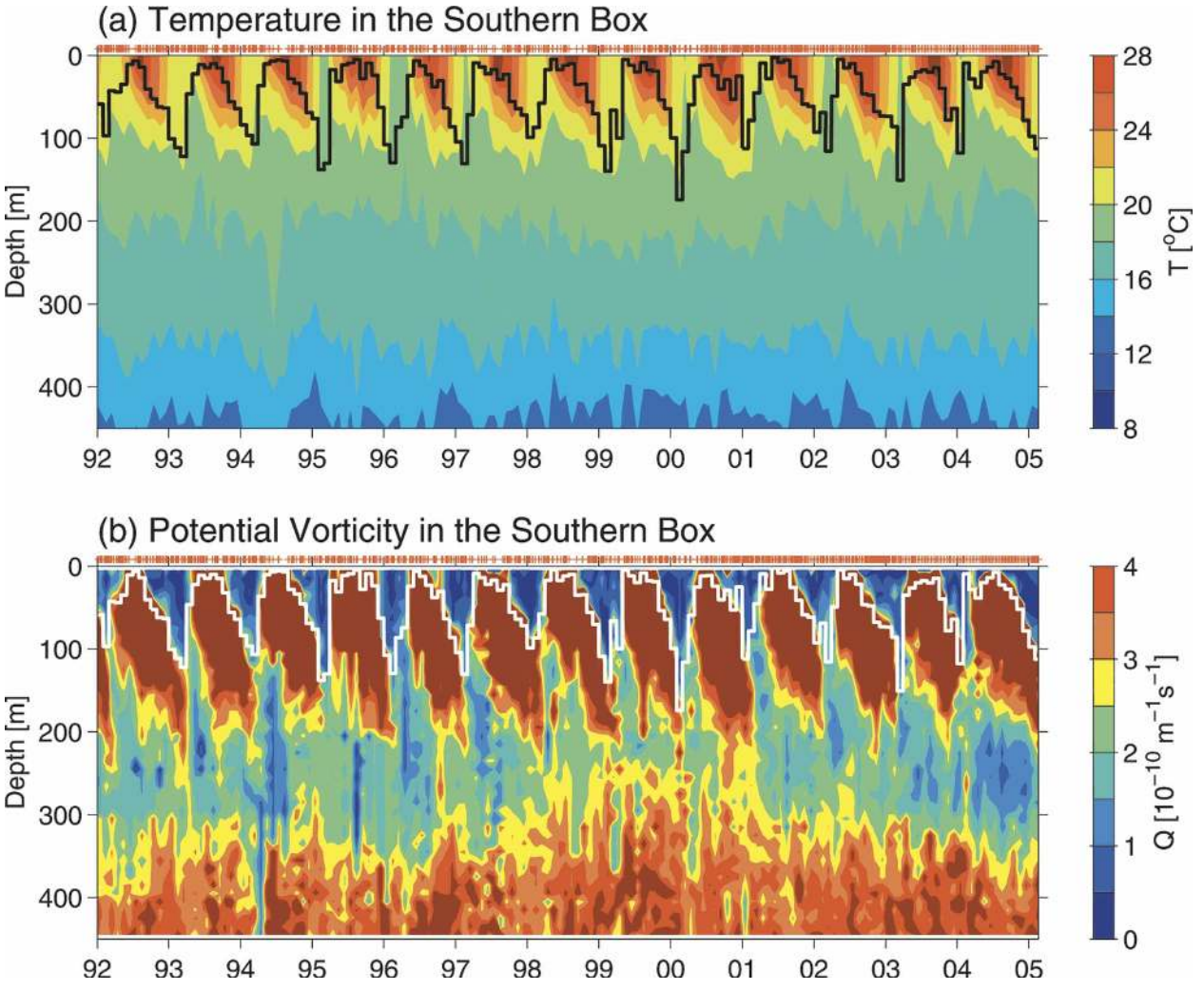

FIG. 7. Same as in Fig. 4 but for the southern box at 26°–30°N and 140°–144°E.

monly has broad spatial scales, this result implies that the decadal mixed layer depth changes seen in the recirculation gyre are likely controlled by processes other than the atmospheric forcing. Quantification of these processes, including the air–sea flux forcing, is pursued in the next section.

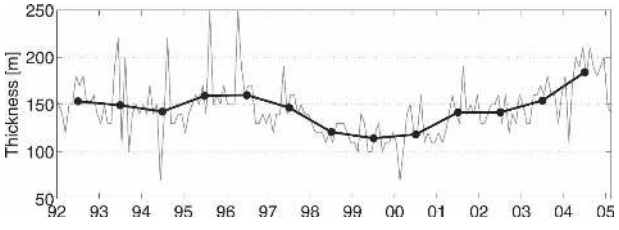

FIG. 8. Time series of the 16°–18°C layer thickness in the region south of the RG. Based on the $T(z, t)$ profiles shown in Fig. 7a. The thick line denotes the annually averaged values.

5. Mechanisms of the decadal STMW changes

As we noted in the introduction, several studies in the past have attributed the variations in the STMW properties to the overlying atmospheric forcing. To test this hypothesis, we plot in Fig. 9a the monthly time series of the net heat flux from the atmosphere to the ocean (Q_{net}) from the NCEP–NCAR reanalysis over the recirculation gyre region (31°–34°N, 141°–150°E). With the removal of the seasonal climatology (the gray curve in Fig. 9a), Fig. 9b shows the time series of the Q_{net} anomalies averaged over the cooling season from November through March. The general trend in Fig. 9b is that positive anomalies (less cooling) are seen in 1993–94, 1997, and 2004, whereas negative anomalies (more intense cooling) prevailed mostly from 1995 to 2003.

In Fig. 10a, we plot the Q_{net} anomalies from the in-

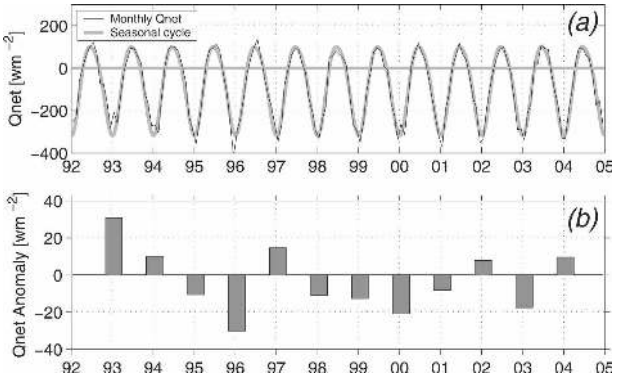

FIG. 9. (a) Time series of the monthly net surface heat flux Q_{net} from NCEP–NCAR reanalysis averaged in the recirculation gyre region of 31°–34°N and 141°–150°E (black line). Gray line denotes the climatological seasonal cycle, (b) Q_{net} anomalies averaged over the cooling season from November through March.

dividual cooling seasons against the observed depths of the late winter mixed layer[2] (defined by the maximum mixed layer depth in each winter shown in Fig. 4a). The correspondence between these two quantities is rather poor. If anything, there appears to be a hint that a positive Q_{net} anomaly (less cooling) corresponds to a thicker, late winter mixed layer depth. This correspondence is counterintuitive, as one would expect that a weaker heat loss at the sea surface should lead to a thinner winter mixed layer.

The decadal variation in the winter mixed layer depth, on the other hand, bears a good resemblance to the low-frequency signals shown in Fig. 2 that reflect the stability of the KE system. Indeed, plotting the late winter mixed layer depth values against the KE pathlengths in the preceding year reveals that a favorable *negative* correlation exists between these two quantities (see Fig. 10b). To understand how the stability of the KE jet is related to the changes in the winter mixed layer depth, it is helpful to realize that a large PV gradient exists between the KE jet and the recirculation gyre. For example, Fig. 11a shows a temperature section across the KE jet measured by the KESS cruise in May 2004 [for details of the cruise, see Qiu et al. (2006)]. STMW in this section is well represented by the shaded 16°–18°C layer south of the KE jet. At the STMW depth (150–400 m), the PV value associated with the baroclinic KE jet is shown in Fig. 11b to be much greater than the low PV value of STMW. When

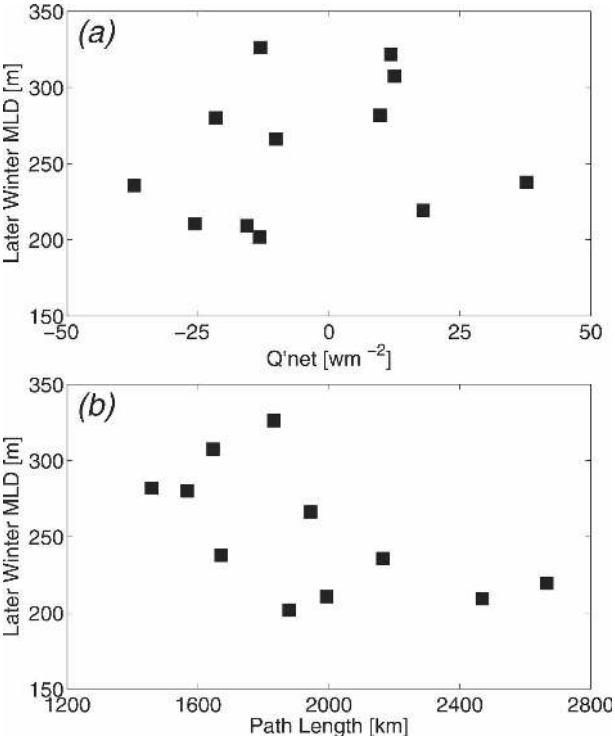

FIG. 10. Scatterplots of (a) the cooling-season (November–March) net surface heat flux anomalies vs the late winter mixed layer depths and (b) the yearly averaged KE pathlengths (see Fig. 2a) vs the late winter mixed layer depths in the following year.

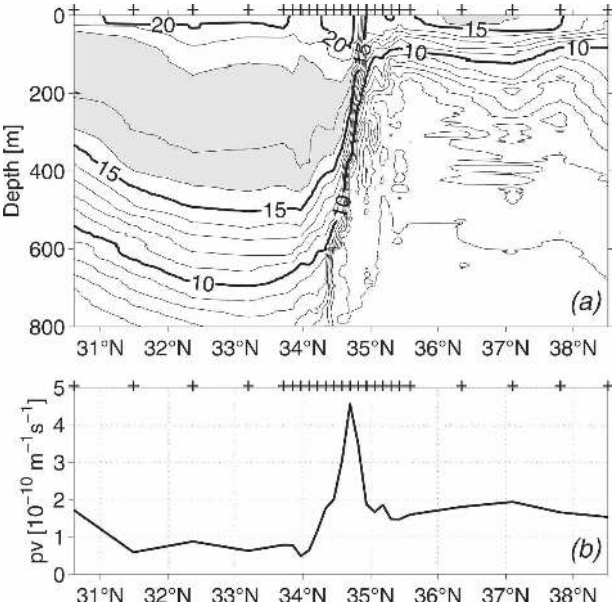

FIG. 11. (a) Meridional potential temperature section across the KE jet from (30.6°N, 143.5°E) to (38.6°N, 147.5°E). Based on CTD measurements from the KESS cruise of May 2004 (Qiu et al. 2006). Areas where $16°C < \theta < 18°C$ are shaded. (b) Values of PV averaged in the depth range of 150–400 m. Crosses at top indicate positions of the available *T/S* profiles.

[2] In this and next sections, signals in the late winter mixed layer depth are used to represent the decadal STMW variations. Use of other indices, such as the 16°–18°C layer thickness of the spring season, will not alter the results qualitatively.

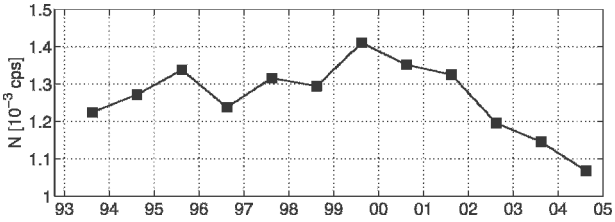

FIG. 12. July–September mean buoyancy frequency N averaged in the surface–450-m layer of the recirculation gyre region. Here, $N = (g\alpha\partial T/\partial z)^{1/2}$, and the $T(z, t)$ profiles are shown in Fig. 4a.

the KE jet is in an unstable state, the high-PV KE water is likely to be mixed into the recirculation gyre through cutoff cold-core eddies (a good example of this can be seen in Fig. 6a). This mixing works to increase the potential vorticity, or equivalently, the stratification frequency N in the recirculation gyre (N is related to potential vorticity Q by $N^2 \equiv g\alpha\partial T/\partial z = gQ/f$).

To explore whether the observed stratification in the recirculation gyre is influenced by the state of the KE system, we plot in Fig. 12 the time series of N averaged in the surface–450-m layer from July to September based on the $T(z, t)$ profiles shown in Fig. 4a. Here, the July–September value is chosen to represent the condition *before* the onset of the cooling season. From Fig. 12, it is clear that N is larger during 1995–2001 when the KE system was in an unstable state, than during 1993–94 and after 2002 when the KE system was in a stable state.

Physically, stratification in the summer/fall months is important because it preconditions the development of the convective mixed layer during the subsequent cooling season. If we initialize the surface ocean stratification by N and let the subsequent surface cooling be $Q_{\text{net}}(t) < 0$, conservation of heat in the surface ocean requires (see Fig. 13)

$$T(-D)D - \int_{-D}^{0} T(z)\,dz = \frac{1}{\rho_o c_p}\int_t Q_{\text{net}}(t')\,dt'. \tag{2}$$

where D is the mixed layer depth, ρ_o is the reference seawater density, and c_p is the seawater heat capacity. When N is assumed to be a constant, the mixed layer depth can easily be solved from Eq. (2):

$$D = \frac{1}{N}\sqrt{\frac{-2\alpha g}{\rho_o c_p}\int_t Q_{\text{net}}(t')\,dt'}. \tag{3}$$

Equation (3) indicates that the depth of the convective mixed layer (i.e., the thickness of wintertime STMW) not only is controlled by the cumulative surface cooling, but also depends on N, the preconditioning stratification. A smaller (larger) N value, found during the stable (unstable) phase of the KE system, will favor development of a deeper (shallower) mixed layer. Indeed, plotting the N values observed in each fall season (the time series in Fig. 12) against the observed mixed layer thickness values in the late winter of the following year reveals a rough inverse relationship between these two quantities (see Fig. 14).

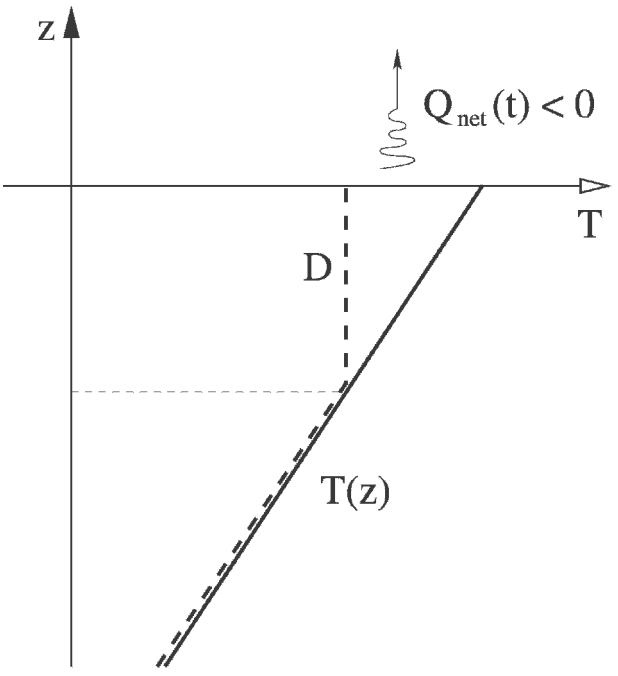

FIG. 13. Schematic illustrating the preconditioning fall stratification (reflected by the initial temperature profile indicated by the thick solid line), the convective mixed layer depth D, and the surface cooling $Q_{\text{net}}(t)$.

From Eq. (3), it is possible to quantify the relative impact of variable N and $\int_t Q_{\text{net}}(t')\,dt'$ on changes in D. By defining $I = \int_t Q_{\text{net}}(t')\,dt'$ and by expanding Eq. (3) in a Taylor series, we have

$$\frac{\delta D}{D} = \left(\frac{N}{D}\frac{\partial D}{\partial N}\right)\frac{\partial N}{N} + \left(\frac{I}{D}\frac{\partial D}{\partial I}\right)\frac{\delta I}{I} + \text{HOT}$$
$$= -\frac{\delta N}{N} + \frac{1}{2}\frac{\delta I}{I} + \text{HOT}. \tag{4}$$

From Figs. 12 and 9, the observed fractional changes in N and I are estimated to be $\delta N/N \sim 7.1\%$ and $\delta I/I \sim 7.2\%$, respectively. (Here, δN and δI are given by their respective rms values.) With these estimates, Eq. (4) suggests that variations in N are about 2 times as effective in modifying the late winter mixed layer depth as those in the cumulative surface cooling.

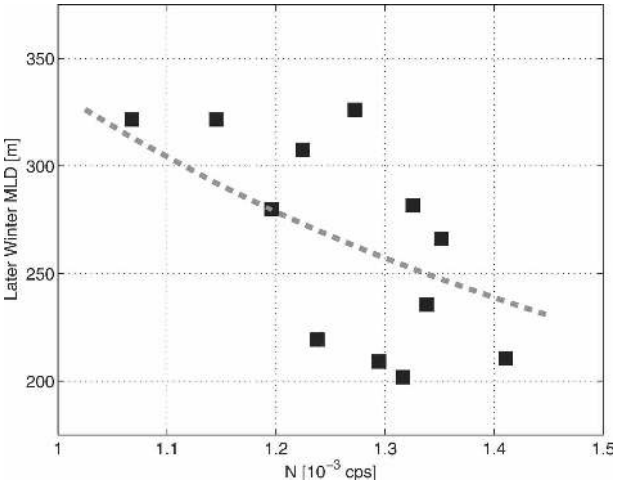

FIG. 14. Scatterplot of July–September mean buoyancy frequency N (see Fig. 12) vs the late winter mixed layer depth D in the following year. Dashed line denotes the best functional fit by ND = const.

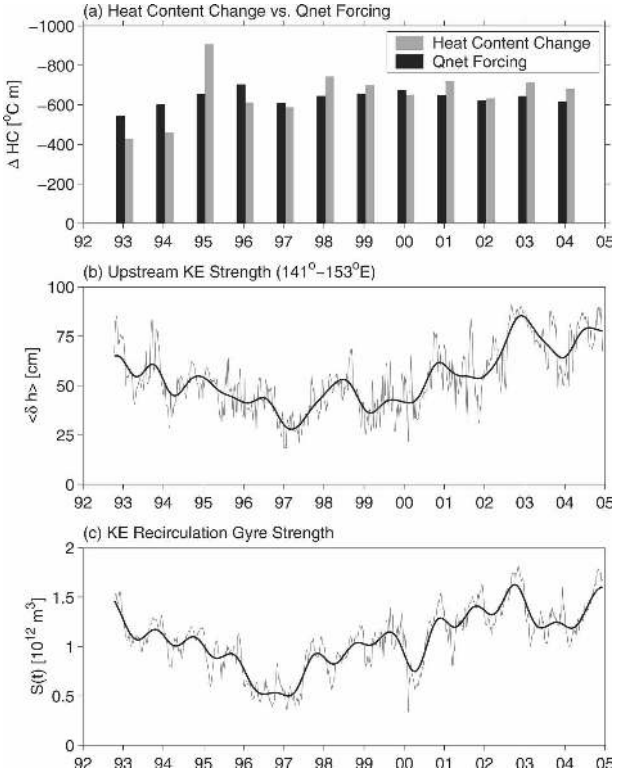

FIG. 15. (a) Heat content change (late March minus early November; gray bars) vs cumulative Q_{net} forcing of November–March (black bars) for individual winters, (b) SSH difference across the KE jet averaged from 141° to 153°E, and (c) strength of the KE recirculation gyre. Panels (b) and (c) are adapted from Qiu and Chen (2005).

6. Effect of lateral oceanic advection

Past studies of STMW variability have also suggested potential roles played by the changes in the surface oceanic circulation (e.g., Yasuda and Hanawa 1997). To examine directly the effect of the time-varying circulation changes, however, requires three-dimensional temperature and flow fields that are unavailable to us. In this section, we attempt to address this issue by using the following *indirect* method.

From the available temperature and surface heat flux data, we assess to what degree the observed upper-ocean heat content change in each winter is controlled by the cumulative surface heat flux forcing. Integrating the temperature equation from the surface to the late winter mixed layer depth ($z = -D$) and over the 5-month cooling season of November–March, we obtain

$$\Delta \int_{-D}^{0} T(z, t)\, dz = \frac{1}{\rho_o c_p} \int_{t} Q_{\text{net}}(t')\, dt' + \text{lateral advection}, \qquad (5)$$

where Δ denotes the difference between late March and early November. The importance of the lateral advection term can be assessed by comparing the heat content change [the lhs of Eq. (5)] with the cumulative surface cooling. Figure 15a shows the comparison between these two terms for the past 12 winters. Here, $T(z, t)$ and D are evaluated from Fig. 4a and the $Q_{\text{net}}(t)$ time series is shown in Fig. 9. The agreement between the heat content change (gray bars in Fig. 15a) and the cumulative surface cooling (black bars) is overall favorable: discrepancies between the two terms are generally less than 10% of the cumulative surface cooling term. The exceptions appear in the first 3 yr, during which the surface heat flux cooling exceeds the heat content change in 1993–94, implying a possible warm advection by the horizontal circulation. In contrast, the heat content change surpasses greatly the cumulative cooling effect in 1995, suggesting the possibility of a cold advection due to the horizontal circulation. It is important to emphasize that the year-to-year difference between the heat content change and the cumulative surface cooling shows little interannual persistence.

To relate the inferred advective effect to the variability of the KE jet, we plot in Fig. 15b the time series of the SSH difference across the KE jet averaged from 141° to 153°E. From the time series, it is clear that the strength of the surface KE jet underwent a clear decadal modulation over the past 12 yr: the jet was strong in 1993–94, had a weakening trend from 1994 to 1997, and strengthened gradually after 1998. Notice that most of this change in the strength of the KE jet was due to the strengthening–weakening of the southern recircula-

tion gyre [Fig. 15c; see Qiu and Chen (2005) for more discussions on this point]. In other words, there existed little *net* surface transport change in the KE system in the period of interest to us. This lack of net surface transport change may explain why there is little interannual persistence in the inferred, year-to-year lateral advection term (Fig. 15a).

It is worth commenting that our finding that STMW formation is enhanced (reduced) when the KE recirculation gyre strengthens (weakens) is *opposite* to that found in Dong (2004). In her study, Dong found more (less) 18° Water is formed when the Gulf Stream is weakened (strengthened). Our findings, on the other hand, agree with the study by Grey et al. (2000) regarding the relationship between the Gulf Stream strength and the volume of 18° Water.

7. Quantification of the oceanic versus atmospheric control

Lack of a clear contribution from lateral advection prompts us to examine the upper-ocean heat balance in more detail. The model of heat conservation used in section 5 is highly idealized: it assumes a constant stratification in the upper ocean and ignores forcing by surface wind stresses. To quantify more realistically the relative importance of N and air–sea flux forcing in controlling the late winter mixed layer depth, we adopt in this section the one-dimensional bulk mixed layer model of Price et al. (1986, hereinafter PWP).

The skill of the PWP model in reproducing observed mixed layer structures in the tropical and midlatitude oceans has been demonstrated by many previous studies (e.g., Schudlich and Price 1992; Plueddemann et al. 1995; Anderson et al. 1996). More recently, this model has been used by Ladd and Thompson (2000) to examine the formation mechanisms for the North Pacific central and eastern mode waters, and by Qiu et al. (2004) to investigate the effects of synoptic-scale atmospheric forcing upon the SST and the mixed layer in the recirculation gyre south of the Kuroshio. The surface mixed layer in the PWP model has constant temperature and velocity, and the wind stress is absorbed evenly within the "slab" mixed layer. Deepening of the mixed layer occurs when the surface ocean is gravitationally unstable or when the bulk Richardson number at the base of the mixed layer is below the critical value 0.65. Vertical mixing in the water column also takes place whenever the local gradient Richardson number falls below the critical value 0.25.

In this study, we carry out four numerical integrations. In the "climatological" run case, the PWP model is initialized with the observed September $N(z)$ profile averaged from 1993 through 2004 and forced subsequently by the 1993–2004 mean daily air–sea flux data of the NCEP–NCAR reanalysis. The model integration ends in May after the surface net heat flux forcing changes from cooling to heating. Salinity effects are not included in this study. Figure 16a shows the comparison between the observed upper-ocean temperature evolution and that modeled from the climatological run. Here, the observed upper-ocean temperature (the left panel in Fig. 16a) is obtained by averaging the monthly $T(z, t)$ profiles shown in Fig. 4a. Overall, the correspondence between the model and observations is favorable and this is particularly true during the deepening phase of the mixed layer (October–March). With the accumulation of a cold bias, the model is less successful in simulating the warming phase of the surface ocean after April. This cold bias is due to the shortcoming of the one-dimensional model, which neglects lateral heat transport. With the annually averaged net surface heat flux in the region being negative, lateral heat advection by the ocean circulation, in fact, must play a role in order to maintain the thermodynamic equilibrium of the surface ocean. As the focus of this study is on the interannually varying depths of the late winter mixed layer, no attempt is made to remove the cold bias seen in the model.

In the "full forcing" runs, the PWP model is initialized with the observed September $N(z)$ profile of each year and forced subsequently by the daily air–sea flux data of the NCEP–NCAR reanalysis until May of the following year. As an example, we plot in Fig. 16b (right panel) the upper-ocean temperature evolution for the period September 2003–May 2004 from the full-forcing run. Favorable correspondence is again seen between the model result and the observed $T(z, t)$ profiles during the deepening phase of the mixed layer (the left panel in Fig. 16b). In comparison with the climatology, both the model and the observations indicate that the SST is colder and the mixed layer depth is deeper in May 2004.

By subtracting the late winter mixed layer depth from the climatological run case, we plot in Fig. 17a (blue curve) the time series of the late winter mixed layer depth anomalies in individual winters. For comparison, the red curve in Fig. 17a shows the observed late winter mixed layer depth anomalies based on Fig. 4a. The observed decadal trend, that is, minimum mixed layer depths in 1998–99 and a deepening trend after 2000, is well captured by the model. The PWP model is less successful in hindcasting the mixed layer depth in the first 3 yr (1994–96) and this is related to the fact that the one-dimensional upper-ocean heat balance in those 3 yr is not as valid (recall Fig. 15a). For brevity,

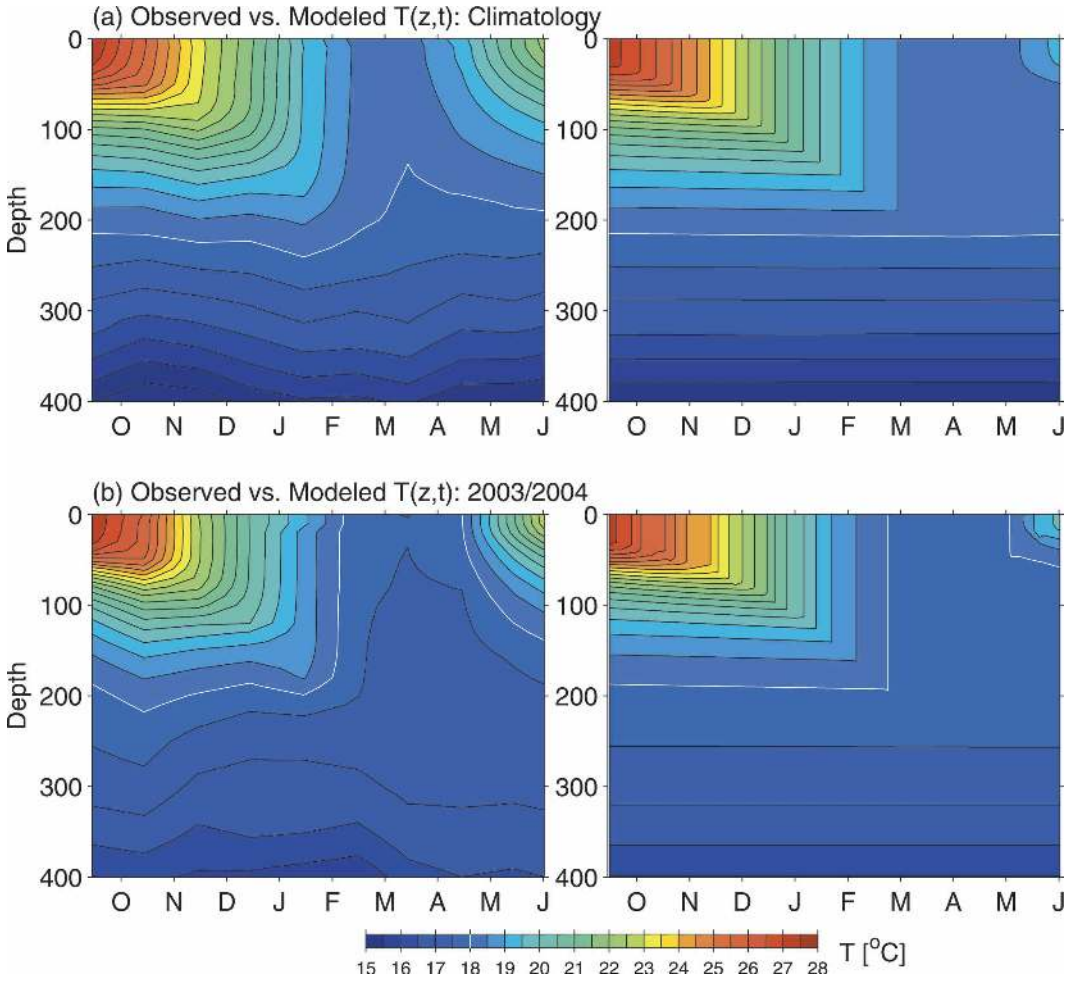

FIG. 16. Upper-ocean temperature evolutions from the (left) observations vs the PWP (right) model runs, with results from (a) the climatological model run and (b) the full-forcing model run for the cooling season of 2003/04. In all panels, contour intervals are 0.5°C and the white contours denote the 18°C isotherms.

the mixed layer depth anomalies from the full-forcing runs will be denoted below as $D_f(t)$, where t signifies individual winters.

To assess the relative importance of the oceanic forcing (through the preconditioning N profile) versus the atmospheric forcing, we conduct two additional model runs. The "oceanic forcing" runs are similar to the full-forcing runs, except that the surface air–sea flux forcing in this case is fixed at the climatological daily values. By design, any changes in the late winter mixed layer depth from the climatology in this case are due to the variations in the preconditioning oceanic state. In Fig. 17b, we plot the late winter mixed layer depth anomalies from the oceanic forcing runs, $D_o(t)$, as the red curve. In the case of the 2003/04 cooling season, the oceanic forcing run predicts a late winter mixed layer deeper than that predicted by the full forcing run (the solid blue curve).

In contrast to the oceanic-forcing runs in which the air–sea flux forcing is climatological, the "atmospheric forcing" runs are driven by interannually varying air–sea flux forcing, but are initialized by the *same* climatological September $N(z)$ profile. In this case, the modeled late winter mixed layer depth anomalies, $D_a(t)$, are solely due to the variations in the overlying atmospheric forcing. The time series of $D_a(t)$ is shown in Fig. 17b as the green curve. In the case of the 2003/04 cooling season, the reduced seasonal cooling (see Fig. 9b) results in a late winter mixed layer depth from the atmospheric-forcing run that is shallower than that of the climatology.

The sum of $D_o(t)$ and $D_a(t)$ is shown in Fig. 17b as the dashed blue curve. Its good agreement with the $D_f(t)$ time series (the solid blue line) indicates that the late winter mixed layer depth anomalies are controlled to a large extent *linearly* by the variations in N and the air–

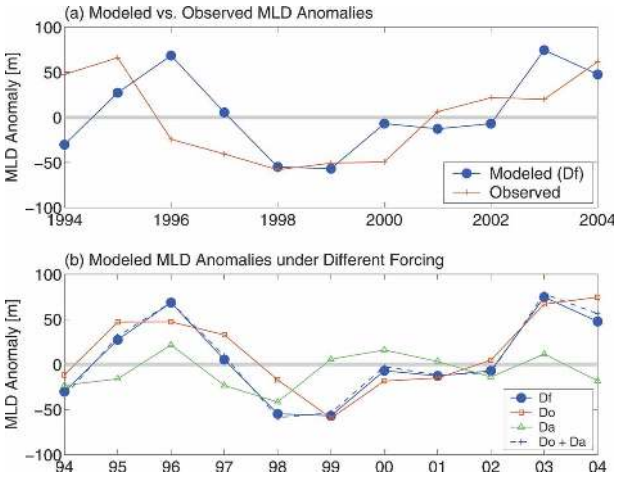

FIG. 17. (a) Comparison between the observed (red pluses) and modeled (blue circles) anomalies of the late winter mixed layer depth and (b) the late winter mixed layer depth anomalies under the different forcing scenarios. Solid blue line shows the result of $D_f(t)$ from the full-forcing run; red line, $D_o(t)$ from the oceanic-forcing run; and green line, $D_a(t)$ from the atmospheric-forcing run. Dashed blue line indicates the sum of $D_o(t)$ and $D_a(t)$. See text for details of the different model runs.

sea flux forcing. Calculation of cross correlations between $D_o(t)$ and $D_f(t)$ and between $D_a(t)$ and $D_f(t)$ reveals that

$$\gamma_{of}^2 \equiv \frac{\langle D_o D_f \rangle^2}{\langle D_o^2 \rangle \langle D_f^2 \rangle} = 0.795 \quad \text{and} \quad \gamma_{af}^2 \equiv \frac{\langle D_a D_f \rangle^2}{\langle D_a^2 \rangle \langle D_f^2 \rangle} = 0.133,$$

respectively. These values imply that changes in the preconditioning N profile are responsible for ~80% of the variance in the $D_f(t)$ time series, whereas the time-varying air–sea flux forcing accounts for ~13% of the variance. This large difference explains the contrasting results presented in Figs. 10a and 10b; namely, while there exists a clear, negative correlation between the KE path variability (which determines the preconditioning N profile) and the late winter mixed layer variability in the following year, no clear connection is found between the signals of the cumulative surface cooling and the late winter mixed layer depth.

8. Summary

Using the available temperature data from XBT, STD, and CTD measurements south of the Kuroshio Extension, we investigated in this study the low-frequency changes in the formation of the North Pacific STMW over the past 12 yr. The focus of the investigation was on the KE recirculation gyre at 31°–36°N and 141°–150°E, corresponding to the central area of the STMW formation. With the aid of concurrent sea surface height information from satellite altimetry, we first identified the temperature profiles that truly sampled waters of the anticyclonic recirculation gyre. With STMW forming close to the KE jet, and with the region of the recirculation gyre being populated with cold-core eddies, this identifying procedure was important in preventing the analyzed temperature profiles from being biased by waters representing the KE jet and the Mixed Water region.

The dominant signal of the STMW variability of the past 12 yr has a clear decadal time scale. It is characterized by a gradual thinning in the late winter mixed layer depth and in the 16°–18°C thermostad layer from 1993 to 1999, and a subsequent steady thickening of these features after 2000. The amplitude of the decadal change is substantial: in contrast to ~200 m during the weak STMW formation years (i.e., 1998/99), the late winter mixed layer depth reaches ~320 m during the enhanced STMW formation years (i.e., 1995/96, 2003/04). For the 16°–18°C thermostad layer beneath the seasonal thermocline, the difference is between ~100 and ~200 m.

Analyses of temperature data to the south of the recirculation gyre (26°–30°N, 140°–144°E) revealed a decadal signal of STMW very similar to that observed in its northern formation region. This attests to the robustness of the decadal STMW signal captured in this study and confirms the notion by many previous studies that STMW, after formation in the recirculation gyres of the Kuroshio and KE, tends to spread south- and southwest-ward into the interior subtropical gyre.

Causes for the observed variability of STMW were sought in 1) the overlying atmospheric conditions, 2) the lateral transport change, and 3) the upper-ocean stratification that preconditions the development of the winter mixed layer. Little correlation is found between the year-to-year anomalies in the cumulative winter-time surface cooling and the depths of the winter mixed layer. This lack of correlation is also reflected in the fact that the late winter mixed layer depth south of the recirculation gyre has a time-varying signal very different from the decadal signal seen in the recirculation gyre. If the atmospheric forcing, which has broad spatial scales, were to cause the decadal STMW variations in the recirculation gyre, one would have expected a similar decadal signal in the winter mixed layer south of the recirculation gyre.

A comparison between the upper-ocean heat content change and the cumulative surface cooling over the winter seasons revealed that these two terms are nearly balanced from 1996 to 2004. Significant differences, however, existed in 1993–95. No clear connection was found between the inferred lateral heat transport (i.e.,

the residual between the upper-ocean heat content change and the cumulative surface cooling) and the decadal changes in the KE jet. This lack of connection is likely related to the fact that the KE system had little *net* surface transport change in the past 12 yr.

The decadal signal of the STMW variability, on the other hand, was found to correlate well with variability in the dynamic state of the KE jet and its southern recirculation gyre. Specifically, during the period of 1997–2001 when the KE system was unstable and the regional level of mesoscale eddy variability was high, less STMW was formed. In the years before 1995 and after 2002 when the KE system was stable with a low regional mesoscale eddy variability, enhanced STMW formation was observed. Changes in the regional eddy variability are able to affect the STMW formation through modifying the fall season stratification within the recirculation gyre: during the unstable state of the KE system, enhanced lateral mixing with the high-PV KE water works to increase the stratification in the recirculation gyre. On the other hand, stratification remains weak when the lateral eddy mixing is suppressed during the stable state of the KE system.

Both a simple upper-ocean heat conservation model and the bulk mixed layer model of Price et al. (1986; PWP) were used in this study to quantify the relative importance of the surface air–sea flux forcing versus the preconditioning stratification in controlling the year-to-year changes in the late winter mixed layer depth. Given the observed air–sea fluxes and the fall stratification profiles of the past 12 yr, both models indicated the dominance of the oceanic contribution through preconditioning. In particular, quantifications using the PWP model under different forcing scenarios revealed that the time-varying preconditioning (air–sea flux forcing) accounts for ~80% (~13%) of the variance in the late winter mixed layer changes. These quantifying values are, of course, pertinent to the period of 1993–2004, during which the KE system was marked by a well-defined decadal oscillation between a stable and an unstable state. It would be interesting for future data analysis and numerical modeling studies to determine how these quantifying values may change over the longer period.

One issue we were not able to address in this study based on the historical temperature dataset is on what time scale mesoscale eddies could alter the upper-ocean stratification in the recirculation gyre. Our preliminary analysis of the profiling *T*/*S* float data from the KESS program indicates that the eddy's high-PV signals are mixed into the recirculation gyre on the intraannual time scale. This result supports the close connection between the level of the eddy variability and the upper-ocean preconditioning emphasized in this study. The detailed process by which mesoscale eddies affect the upper-ocean stratification of the recirculation gyre will be reported upon in a future study.

Acknowledgments. This study benefited from fruitful discussions with Ted Durland, Kimio Hanawa, Mark Merrifield, Toshio Suga, and Niklas Schneider. Detailed comments made by Lynne Talley and the anonymous reviewers helped to improve an early version of the manuscript. The temperature profile data were generously provided by the National and Japan Oceanographic Data Centers (NODC and JODC), the Argo profiling float data by the U.S.–GODAE Argo Global Data Assembly Center, the surface wind stress and heat flux data by the National Centers for Environmental Prediction, and the merged T/P, *Jason-1*, and *ERS-1/2* altimeter data by the CLS Space Oceanography Division as part of the Environment and Climate EU ENACT project. This study was supported by NASA through Contracts 1207881 and 1228847.

REFERENCES

Anderson, S. P., R. A. Weller, and R. B. Lukas, 1996: Surface buoyancy forcing and the mixed layer of the western Pacific warm pool: Observation and 1D model results. *J. Climate,* **9,** 3056–3085.

Argo Science Team, 2001: Argo: The global array of profiling floats. *Observing the Oceans in the 21st Century,* C. J. Koblinsky, and N. R. Smith, Eds., GODAE Project Office, 248–258.

Bingham, F. M., 1992: Formation and spreading of Subtropical Mode Water in the North Pacific. *J. Geophys. Res.,* **97,** 11 177–11 189.

——, T. Suga, and K. Hanawa, 1992: Comparison of upper ocean thermal conditions in the western North Pacific between two pentads: 1938–42 and 1978–82. *J. Oceanogr.,* **48,** 405–425.

Conkright, M. E., R. A. Locarnini, H. E. Garcia, T. D. O'Brien, T. P. Boyer, C. Stephens, and J. I. Antonov, 2002: *World Ocean Atlas 2001: Objective Analyses, Data Statistics, and Figures, CD-ROM Documentation.* National Oceanographic Data Center, Silver Spring, MD, 17 pp.

Dong, S., 2004: Interannual variations in upper ocean heat content and heat transport convergence in the western North Atlantic. Ph.D. thesis, University of Washington, 141 pp.

Ducet, N., P.-Y. Le Traon, and G. Reverdin, 2000: Global high-resolution mapping of ocean circulation from TOPEX/Poseidon and *ERS-1* and *-2*. *J. Geophys. Res.,* **105,** 19 477–19 498.

Grey, S. M., K. Haines, and A. Troccoli, 2000: A study of temperature changes in the upper North Atlantic: 1950–94. *J. Climate,* **13,** 2697–2711.

Hanawa, K., and J. Kamada, 2001: Variability of core layer temperature (CLT) of the North Pacific subtropical mode water. *Geophys. Res. Lett.,* **28,** 2229–2232.

——, and L. D. Talley, 2001: Mode waters. *Ocean Circulation & Climate: Observing and Modelling the Global Ocean,* G.

Siedler, J. Church, and J. Gould, Eds., Academic Press, 373–386.

Huang, R.-X., and B. Qiu, 1994: Three-dimensional structure of the wind-driven circulation in the subtropical North Pacific. *J. Phys. Oceanogr.,* **24,** 1608–1622.

Jenkins, W. J., 1982: On the climate of a subtropical gyre: Decade timescale variations in water mass renewal in the Sargasso Sea. *J. Mar. Res.,* **40** (Suppl.), 427–464.

Kistler, R., and Coauthors, 2001: The NCEP–NCAR 50-Year Reanalysis: Monthly means CD-ROM and documentation. *Bull. Amer. Meteor. Soc.,* **82,** 247–267.

Ladd, C., and L. Thompson, 2000: Formation mechanisms for North Pacific central and eastern subtropical mode waters. *J. Phys. Oceanogr.,* **30,** 868–887.

Le Traon, P.-Y., and G. Dibarboure, 1999: Mesoscale mapping capabilities of multiple-satellite altimeter missions. *J. Atmos. Oceanic Technol.,* **16,** 1208–1223.

Luyten, J. R., J. Pedlosky, and H. Stommel, 1983: The ventilated thermocline. *J. Phys. Oceanogr.,* **13,** 292–309.

Masuzawa, J., 1969: Subtropical mode water. *Deep-Sea Res.,* **16,** 463–472.

——, 1972: Water characteristics of the North Pacific central region. *Kuroshio—Its Physical Aspects,* H. Stommel and K. Yoshida, Eds., University of Tokyo Press, 95–127.

Mizuno, K., and W. B. White, 1983: Annual and interannual variability in the Kuroshio Current system. *J. Phys. Oceanogr.,* **13,** 1847–1867.

Plueddemann, A. J., R. A. Weller, M. Stramska, T. D. Dickey, and J. Marra, 1995: Vertical structure of the upper ocean during the Marine Light-Mixed Layers experiment. *J. Geophys. Res.,* **100,** 6605–6619.

Price, J. F., R. A. Weller, and R. Pinkel, 1986: Observations and models of the upper ocean response to diurnal heating, cooling, and wind mixing. *J. Geophys. Res.,* **91,** 8411–8427.

Qiu, B., and S. Chen, 2005: Variability of the Kuroshio Extension jet, recirculation gyre, and mesoscale eddies on decadal timescales. *J. Phys. Oceanogr.,* **35,** 2090–2103.

——, ——, and P. Hacker, 2004: Synoptic-scale air–sea flux forcing in the western North Pacific: Observations and its impact on SST and the mixed layer. *J. Phys. Oceanogr.,* **34,** 2148–2159.

——, P. Hacker, S. Chen, K. A. Donohue, D. R. Watts, H. Mitsudera, N. G. Hogg, and S. R. Jayne, 2006: Observations of the subtropical mode water evolution from the Kuroshio Extension System Study. *J. Phys. Oceanogr.,* **36,** 457–473.

Schudlich, R. R., and J. F. Price, 1992: Diurnal cycles of current, temperature, and turbulent dissipation in a model of the equatorial upper ocean. *J. Geophys. Res.,* **97,** 5409–5422.

Suga, T., and K. Hanawa, 1995a: The Subtropical Mode Water circulation in the North Pacific. *J. Phys. Oceanogr.,* **25,** 958–970.

——, and ——, 1995b: Interannual variations of North Pacific Subtropical Mode Water in the 137°E section. *J. Phys. Oceanogr.,* **25,** 1012–1017.

——, ——, and Y. Toba, 1989: Subtropical mode water in the 137°E section. *J. Phys. Oceanogr.,* **19,** 1605–1618.

Talley, L. D., 1985: Ventilation of the subtropical North Pacific: The shallow salinity minimum. *J. Phys. Oceanogr.,* **15,** 633–649.

——, and M. Raymer, 1982: Eighteen-degree water variability. *J. Mar. Res.,* **40** (Suppl.), 757–775.

Taneda, T., T. Suga, and K. Hanawa, 2000: Subtropical mode water variation in the southwestern part of the North Pacific subtropical gyre. *J. Geophys. Res.,* **105,** 19 591–19 598.

Teague, W. J., M. J. Carron, and P. J. Hogan, 1990: A comparison between the Generalized Digital Environmental Model and Levitus climatologies. *J. Geophys. Res.,* **95,** 7167–7183.

Yasuda, T., and K. Hanawa, 1997: Decadal changes in the mode waters in the midlatitude North Pacific. *J. Phys. Oceanogr.,* **27,** 858–870.

——, and ——, 1999: Composite analysis of North Pacific subtropical mode water properties with respect to the strength of the wintertime East Asian monsoon. *J. Oceanogr.,* **55,** 531–541.